

## Article

# Cryogels with Noble Metal Nanoparticles as Catalyst for “Green” Decomposition of Chlorophenols

Dmitriy A. Berillo<sup>1,2,\*</sup>  and Irina N. Savina<sup>1</sup> <sup>1</sup> School of Applied Sciences, University of Brighton, Huxley Building, Lewes Road, Brighton BN2 4GJ, UK<sup>2</sup> MINES ParisTech, PSL Research University, Center for Materials Forming (CEMEF), UMR CNRS 7635, CS 10207, 06904 Paris, France

\* Correspondence: dmitriychemist@gmail.com

**Abstract:** Pollution of the aquatic environment by halogen derivatives widely used as antiseptic compounds, as well as chemicals for various industrial purposes, is significant. Existing systems of bioremediation poorly solve the problem of eliminating pollution. This paper discusses the preparation of novel macroporous chitosan-based cryogels with in situ-immobilized Pd or Pt nanoparticles as a catalyst for dichlorination reactions. The formation mechanism of metal coordinated chitosan gels using Medusa software modelling and rheology ( $G'$  and  $G''$ ) is discussed. Metal coordinated chitosan gels were subsequently converted into covalently cross-linked macroporous cryogels with in situ-immobilized Pd or Pt nanoparticles using the redox potentials difference of the reaction mixture. Noble metal nanoparticles of average size, 2.4 nm, were evenly distributed in the cryogel structure. The effectiveness of these gels as a catalyst for the decomposition of chloro-compounds o-chlorophenol, p-chlorophenol and 2,4-dichlorophenol was tested. The catalytic hydrogenation reaction was carried out using the “green reducing agent” formic acid. Increasing the excess of formic acid with heating increases the degree of conversion up to 80–90%. The CHI-GA-PdNPs cryogel at pH 6 showed better efficiency in the hydrogenation process compared to the CHI-GA-PtNPs cryogel; however, no significant difference in the degree of conversion at pH 3 was observed. The termination of a catalytic reaction in a batch mode have been studied. Several control tests were carried out to elucidate the mechanism of catalyst poisoning. The presented catalytic system may be of interest for studying reactions in a flow through mode, including the reactions for obtaining valuable chemicals.

**Keywords:** PdNPs; PtNPs; catalysis; metal coordination; chlorophenols; chitosan



**Citation:** Berillo, D.A.; Savina, I.N. Cryogels with Noble Metal Nanoparticles as Catalyst for “Green” Decomposition of Chlorophenols. *Inorganics* **2023**, *11*, 23. <https://doi.org/10.3390/inorganics11010023>

Academic Editors: Franz Edwin López Suárez, Robison Buitrago and Andres F. Suárez

Received: 5 December 2022

Revised: 28 December 2022

Accepted: 30 December 2022

Published: 2 January 2023



**Copyright:** © 2023 by the authors. Licensee MDPI, Basel, Switzerland. This article is an open access article distributed under the terms and conditions of the Creative Commons Attribution (CC BY) license (<https://creativecommons.org/licenses/by/4.0/>).

## 1. Introduction

Drinking water and water for agriculture are an important resource for life and the environment. Today, the agricultural sector continues to use reliable, persistent chloroderivatives in herbicides, fungicides, coolants and insulating fluids (transformer oil) for transformers and capacitors [1–3]. WHO pays special attention to the limits of these compounds in drinking water. Guideline values (GV) established for 17 territories and 60 countries are 70 µg/L and 60 µg/L for tetrachloroethene, 1,2-dichloroethane, sodium dichloroisocyanurate, and dibromoacetonitrile; 20 µg/L for dichloroacetonitrile, 0.3 µg/L and 0.5 µg/L for vinyl chloride [4]. The European Union has set target limits of 0.1 µg/L for maximum concentrations of pesticides and their degradation products and 0.5 µg/L for total concentrations of pesticides in the environment [4,5]. Contamination of groundwater with chlorophenols ranges from 0.15–100 mg/L [5,6]. Exposure to chlorophenols has been associated with industries producing textiles, leather products, household preservatives, and the petrochemical industry [7–9]. The International Agency for Research on Cancers has divided chlorophenols into the following five groups: pentachlorophenol (PCP), 2,3,4,6-tetrachlorophenol (2,3,4,6-TeCP); 2,4,6-trichlorophenol (2,4,6-TCP), 2,4,5-trichlorophenol (2,4,5-TCP) and 2,4-dichlorophenol (2,4-DCP), belonging to 2B group of potential human carcinogens [3]. Trichlorophenol was found in

the blood serum and urine of sawmill workers at concentrations ranging from 206 to 1186  $\mu\text{g/L}$  and 196 to 2320  $\mu\text{g/L}$ , respectively [3]. *o*-Chlorophenol (2CP) is used as a precursor in the production of higher chlorophenols and dyes, and as a preservative [10]. Chlorophenols typically have very low organoleptic thresholds, for example taste and odour thresholds levels in water for 2CP are 0.1  $\mu\text{g/L}$  and 10  $\mu\text{g/L}$ , respectively. Monitoring of Canadian wastewater treatment plants identified 40 plants with elevated levels of chlorophenol in drinking water during chlorination process with concentrations of 2CP (maximum 65 ng/L), 2,4-DCP (72 ng/L), and 2,4,6-TCP (719 ng/L), respectively [11]. Water collected from the Huang-Bo Sea in Dalian, China showed that concentrations of halogenated phenols, polybrominated diphenyl ethers and polybrominated diphenyl ethers were 77.2–168.5 ng/L, 5.30 ng/L and 0.08–0.88 ng/L, respectively [10]. All these examples clearly demonstrate the severity of the problem of water pollution by chlorophenol compounds and the need to develop methods for removing these compounds from water. There are several hydrodechlorination approaches that use an expensive catalyst based on palladium and rhodium supported on carbon (Pd/C and Pd/Rh/C). For example, the decomposition of 2,3,5-trichlorophenol in the presence of (Pd/C and Pd/Rh/C) was accelerated by increasing the percentage of methanol in the water/methanol mixture to 50% (*v/v*) and higher. The hydrodechlorination activity of catalysts was in the order Pd/C > Pd/Rh/C > Rh/C [10]. Chloroderivatives at a concentration of 100 ppm can be completely degraded within 2 h using a 3% Pd/graphene oxide catalyst [12]. A palladium nanocatalyst supported on a fibrous nano-silica showed good catalytic activity in the reduction of 4-nitrophenol and hydrodechlorination of 4-chlorophenol (4CP) in an aqueous solution under mild conditions [13]. Porous carbon catalyst (SMK-3) was obtained by pyrolysis of SBA-15 silica impregnated with a commercial resol resin, followed by impregnation with PdNPs. The undoped and nitrogen-doped SMK-3 carbon were used for catalysis. It showed rapid hydrodechlorination of 4CP by hydrogen with exceptional selectivity for phenol conversion. Optimum activity was noted at 30 °C for a catalyst with a nitrogen-doped support (76–81 mmol·g Pd<sup>-1</sup>·min<sup>-1</sup>) [14]. Significant achievement in the de-chlorination of chlorophenols to safer compounds has been made using catalysts together with hydrogen gas. However, the use of hydrogen gas can be dangerous due to leakage due to its small size and high penetration ability and ability to form explosive mixtures with air. Kopinke's research group illustrated possibility of use of formic acid, isopropanol and hydrazine as reducing agents for the Pd-catalyzed hydrodechlorination of chlorobenzene in water at ambient temperature [15]. PdNPs immobilised on multi-walled carbon nanotubes (Pd/MWCNTs) were also successfully utilised for hydrodechlorination of 4CP. The efficiency of the process is significantly affected by the size of the loaded Pd nanoparticles: an increase in the size of the nanoparticles reduces the percentage of 4CP removal, so for Pd particles of 6.4, 9.5, and 13.1 nm, the percentage of removal was 100, 60, and 29%, respectively [16]. In situ, 6.5 nm PdNPs prepared by ascorbic acid reduction and stabilised with carboxymethylcellulose showed comparable catalytic activity in trichloroethene de-chlorination (with  $K_{\text{obs}}$  up to 692 L g<sup>-1</sup> min<sup>-1</sup>) with PdNPs synthesized using the conventional borohydride reduction method [17].

However, there are also inexpensive options, such as using a catalyst and sunlight. Complete degradation of 0.1 L 25 ppm 2CP was achieved in the presence of g-C<sub>3</sub>N<sub>4</sub>, TiO<sub>2</sub> and TiO<sub>2</sub>/g-C<sub>3</sub>N<sub>4</sub> hybrid nanocatalysts after 125, 110 and 65 min of sun exposure, respectively [7]. Double perovskite La<sub>2</sub>FeTiO<sub>6</sub> showed better photocatalytic activity than that of single perovskite LaFeO<sub>3</sub>, having a 4CP degradation of 62.1% after 5 h of sun light irradiation [17]. A study of TCP photodegradation using various copper particles on a multi-copper hybrid catalyst showed that the highest concentration of Cu between layers had the highest TCP photodegradation conversion of 95% [18]. Spills of 2CP into the environment and wastewater from various plants can be cleaned up cheaply with metallurgy waste such as iron dust or iron sand particles combined with aeration [19]. The use of hydrogen gas is one of the most conventional, cheap and scalable catalytic processes. Nevertheless, an alternative way to avoid the use of hydrogen gas is the catalytic decomposition of formic

acid (FA), which has been used to dehalogenate organic compounds [2,20]. However, this approach has only been tested with catalyst suspension, which requires subsequent separation, which can be problematic when fine catalyst particles are used. Bioremediation of phenols and chlorophenols using columns with cross-linked viable bacterial cells is applicable, but the kinetic rate is low at concentrations above 25 ppm [21,22]. Cryogels—macroporous polymers with a well-developed system of channels—were used to purify water from various harmful metal ions and some dyes. A device for microextraction based on chitosan (CHI) cryogel has recently been proposed for the isolation and enrichment of heavy metal ions ( $\text{Cu}^{2+}$ ,  $\text{Cd}^{2+}$  and  $\text{Pb}^{2+}$ ) in situ [23]. Removal of arsenic from water has been shown using a recyclable cross-linked chitosan cryogel doped with metal oxide [24]. Another study investigated chitosan/glycidyl methacrylate cryogels for efficient removal of cationic and anionic dyes [25]. Chitosan cryogels decorated with silver nanoparticles were tested for water disinfection [26]. Previously, we illustrated the synthesis of chitosan-based cryogels with in situ synthesized impregnated PdNP and AuNP, which show a high efficiency of nitrophenol reduction by borohydride and also the oxidation of benzaldehyde derivatives in aerated water [27–29]. Some researchers have shown the possibility of using immobilized peroxidase enzymes on cryogel to decompose phenol derivatives, but this approach is expensive [30]. In this study, an advanced PdNPs catalyst supported on macroporous hydrogel was developed for a hydrogen-free catalytic de-chlorination process. The degradation of chlorophenol was carried out in a catalytic column containing immobilized PdNPs using a formic acid salt as a “green reducing agent”, which converted to hydrogen in situ.

## 2. Materials and Methods

### 2.1. Materials

Sodium tetrachloropalladate (II) (98%), palladium chloride(II) ( $\text{PdCl}_2$ ) and potassium tetrachloroplatinate  $\text{K}_2[\text{PtCl}_4]$  (98%) were obtained from Aldrich Chem. Co. (Milwaukee, WI, USA).  $\text{Na}_2[\text{PdCl}_4]$  solutions were synthesized by known methods involving dissolution from palladium (II) chloride  $\text{PdCl}_2$  in sodium chloride. Medium viscosity chitosan with a degree of acetylation of 85%, 2CP, 4CP and 2,4-dichlorophenol (2,4DiCIPh, 99%) were obtained from Aldrich (Steinheim, Germany). Formic acid (FA) (99%) and sodium borohydride (98%) were obtained from Fluka (Steinheim, Germany). Sodium acetate trihydrate was provided by Merck (Darmstadt, Germany).

### 2.2. Catalyst Cryogel Preparation

The catalyst based on PdNPs was prepared as previously described [28]. Briefly, chitosan (CHI) was dissolved in 0.2 M aqueous acetic acid. A certain amount of 0.0145 M  $\text{Na}_2[\text{PdCl}_4]$  solution (0.07–0.28 mL) was added to 1.1 (% w/v) CHI to obtain final concentration of Pd 0.05, 0.2, 0.4 and 0.6 mM, stirred vigorously, and frozen at  $-12\text{ }^\circ\text{C}$  in a cryobath. After freezing for 18–24 h, the samples were thawed at room temperature and transferred to a 2.5% GA solution in 0.1 M phosphate buffer (pH 7.4). The cryogels were incubated at room temperature for 3 h and then extensively washed with water to remove unreacted GA and the obtained chemically cross-linked cryogels containing PdNPs were named as CHI-GA-PdNPs.

### 2.3. Mechanical Properties of the Scaffold

The elastic modulus of the cryogel were studied using a Texture analyser TA-XT2 instrument (Stable Micro Systems, Godalming, Surrey, UK). The compression test was performed at room temperature. The trigger force was set at 1g and the loading (compression) 50 g at a speed of 0.05 mm/s. The elastic modulus was calculated at a deformation of 5% using the equation:

$$E = (F/S)/(\Delta h/h)$$

where E is the elastic modulus (Pa), F is the force applied (N), S is the cross-sectional area of the sample ( $\text{m}^2$ ),  $\Delta h$  is the height (m) at compression, and h is the original height (m).

#### 2.4. Fourier-Transform Infrared Spectroscopy (FTIR)

Freeze dried cryogels CHI-GA-PdNPs and CHI-GA were studied using Universal ATI FTIR spectroscopy (Perkin Elmer, Spectrum 650, Waltham, MA, USA). FTIR spectra were obtained in the range of 4000–650  $\text{cm}^{-1}$  during 128 scans, with 2  $\text{cm}^{-1}$  resolution, using diffuse reflectance mode.

#### 2.5. Transmission Electron Microscopy (TEM)

TEM was used to analyse PdNPs incorporated in the cryogels wall. Transmission electron microscopy (JEOL JEM1400-Plus Transmission Electron Microscope operated at 120 kV equipped with a Gatan OneView camera (4 k × 4 k) (Jeol, Tokyo, Japan) was used. Freeze dried cryogel was submerged in TAAB 812 resin. The embedding was carried out gradually, using two 5 min rinses in epoxy propane, and then every hour the amounts of TAAB 812 in epoxy propane was increased as follows: 33%, 50%, 100%. Blocks were polymerized in an oven at 60 °C for 24 h. Then, a thin slice of the cryogel with a width in the range of 0.12–0.2  $\mu\text{m}$  was cut by the Reichert Ultracut E microtome (Reichert-Jung, Vienna, Austria). The slice was placed on a Quantifoil holey carbon copper grids (Quantifoil Micro Tools GmbH, Cu 200 R2/1, (Agar Scientific, Stansted, Essex, UK) and the samples were incubated at room temperature overnight [29]. TEM microphotographs image analysis was performed using Image J software. The area of the various shapes of PdNPs was used to calculate the dependence of the number of particles vs. PdNPs size. The area of the circle was converted into diameter applying a well-known equation  $D = 2 \times (S/\pi)^{1/2}$ .

#### 2.6. Scanning Electron Microscopy (SEM)

To preserve the original structure of the cryogel for scanning electron microscopy, the samples were freeze-dried and thin discs 1–2 mm thick were manually cut out. Pt layer was sputtered using a Quorum (Q150TES) coater. Samples were scanned using a Zeiss Sigma field emission gun SEM (Zeiss NTS). SEM images were obtained with a Carl Zeiss Leo 1450VP SEM with an Oxford Instruments Energy Dispersive Spectrometer using following settings: accelerating voltage 10.00 kV; magnification: 15,503×; working distance: 8.5 mm; specimen tilt (degrees) 0.0; elevation (degrees) 35.0; azimuth (degrees) 0.0; number of channels: 1024; energy range 20 keV; energy per channel 20.0 eV; detector type Id:12; detector type: X-Max; window type: SATW.

#### 2.7. Thermogravimetric Analysis (TGA)

Composite cryogels containing PdNPs were characterized using TGA (Q500 analyser from TA Instruments). The composite cryogel and control samples (cryogel without particles) were analysed in an atmosphere of air and nitrogen during heating from 40 to 500 °C at heat flow 10 °C/min. For all samples, the TGA method Ramp was applied.

#### 2.8. Catalytic Activity of Containing PdNPs

The catalytic activity of PdNPs supported on chitosan-glutaraldehyde cryogel containing various amounts of PdNPs (0.05, 0.2 and 0.4 mM) was studied in batch mode at room temperature (22 °C). The catalytic reaction was adopted from an earlier report and carried out in a 20 mM FA solution at pH 3 [31]. CHI-GA-PdNPs 0.2 mM cryogel (0.231 g wet weight) was added to 15–20 mL of 0.4 mM 2CP dissolved in FA (20–40 mM). The solution was degassed and properly closed with a septum. The catalytic degradation of chlorophenol was carried out in glass vessels under a nitrogen atmosphere. At each time point, 0.5 mL of 2CP solution was withdrawn from the reaction vessel for UV analysis and stored at 4 °C for HPLC. The calibration curve equation for estimating 2CP concentration using UV spectroscopy at 280 nm was  $y = 0.5074x + 0.0176$  (Figure S7). In the control experiment with CHI-GA cryogel, no adsorption of 2CP was detected.

### 2.9. HPLC analysis of Chlorophenols

Final concentrations of chlorophenol and derivatives in water after the catalytic degradation were estimated using an Agilent 1100 HPLC using a UV detector at 280 nm. Samples were filtered through 0.22 µm filter membranes prior to HPLC analysis. A C18 reverse phase column was used, and the mobile flow rate phase was 1 mL/min.

The HPLC method was as follows. Acetic acid 1% *v/v* in water (C) and methanol (D) was used as the mobile phase. The column and sample temperatures were 45 °C and 25 °C, respectively; (C) gradients start at 75.0, end at 44.0%; (D) gradient starts at 25.0, end at 56.0% over 9.5 min, and at composition 44–56% C-D over 5 min; (C) gradient start at 44.0, end at 0% with a duration of 1.0 min and (D) gradient starts at 56.0%, end at 100.0%, over 1.0 min. It was kept for 5 min at 100% of CH<sub>3</sub>OH and 1% HAc. (C) gradient starts at 0, ends at 75.0% over 1.0 min; (D) gradient starts at 100.0%, ends at 25.0% with a duration of 1.0 min [21].

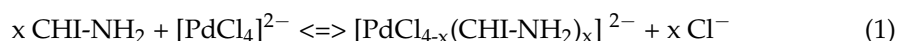
### 2.10. Gas Chromatography-Mass Spectrometry (GC-MS)

The products of the dehalogenation reaction were analysed using electron impact gas chromatography-mass spectrometry and a quadrupole analyzer (GC-EI-MS, Agilent model 7890, Agilent Technologies, Santa Clara, CA, USA) [32]. A BPX5 fused-silica capillary column of 30 m × 0.25 mm I.D. with a film thickness of 0.25 µm and a stationary phase of 5% phenyl polysilphenylene-siloxane (SGE Analytical Science, Milton Keynes, UK) was used for separation, which was carried out with helium at a flow rate of 1 mL min<sup>-1</sup>. The injection temperature was 250 °C. The oven temperature program included 2 min at 50 °C with an increase to 250 °C at a rate of 20 °C min<sup>-1</sup>. The injection volume was 1 µL with a split ratio of 1:2.

## 3. Results and Discussion

### 3.1. Cryogel Characterization

Cryogel is a macroporous polymer material with a unique structure of interconnected pores, which provide high permeability and a large surface area for the adsorption and breakdown of contaminants [25,26,29]. A 1.1% CHI solution potentially contains 58 mM of primary amino groups that can participate in ligand exchange with noble metal complexes according to Equation 1 (Figure 1). It is assumed that the reactivity of primary amino group is comparable to ammonia cation.



According to the simulation data in the Medusa software, the Pd ion speciation at pH above 5.5 the highest concentration of Na<sub>2</sub>[Pd(NH<sub>3</sub>)<sub>4</sub>] complex is observed, these data correlate well with the rheology data and the observed rapid gel formation at pH 5.6. At the same time, a liquid solution of CHI and Na<sub>2</sub>[PdCl<sub>4</sub>] at 0.2–0.6 mM at pH 4.5 did not lead to hydrogel formation over time. Therefore, the cryogel formation is associated with cross-linking of CHI chains through formation of a multidentant chelate. There is also an instant electrostatic interaction between the protonated amino groups and the palladium complex (Equations (2) and (3)).

The CHI-[PtCl<sub>4</sub>] cryogel is stable in the pH range from 5 to 12 and dissolves slowly in acidic pH due to a reversible ligand exchange reaction. It is interesting to note that no ligand exchange occurred when potassium tetrachloroplatinate K<sub>2</sub>[PtCl<sub>4</sub>] was used. The modeling complex correlates well with the literature data and experimental results (Figure 2A). For instance, there is no formation of cis-platin in direct interaction of K<sub>2</sub>[PtCl<sub>4</sub>] with ammonium [33]. Therefore, the formation of CHI cryogel was induced by electrostatic interactions only between tetrachloroplatinate and positively charged amino groups of

CHI. This explains the 10-fold difference in cross-linker concentration for gel formation compared to the palladium complex. Even if there will be a different ligand such as glycine, the ligand exchange process will not occur (Figure 2B).

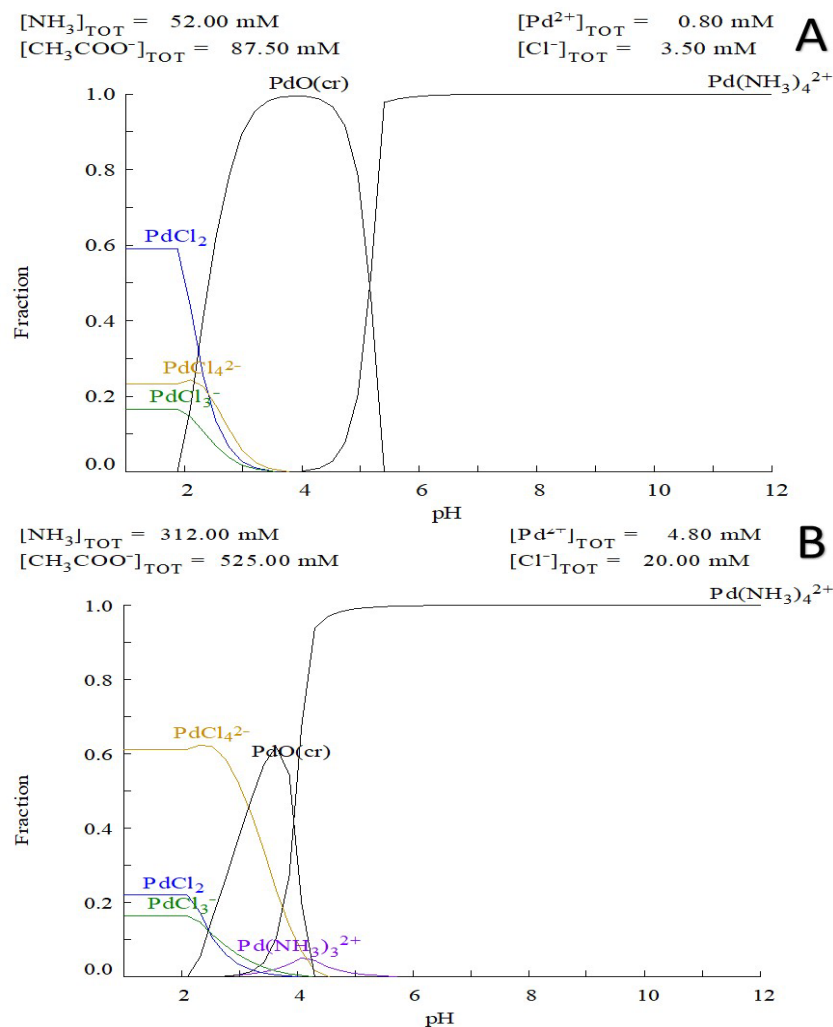


**Figure 1.** Speciation of palladium ions in the reaction mixture solution of: (A) 0.8 mM Pd(II) ions, 52 mM ammonia, 87.5 mM of acetic acid and 3.5 mM chloride anion vs pH; (B) 4.8 mM Pd(II) ions 312 mM ammonia, 525 mM of acetic acid and 20 mM chloride anion modeling the higher concentration in of cross-linking agent in frozen state (Diagram created by Medusa software).

The reaction mixture of 0.4 mM  $\text{Na}_2[\text{PdCl}_4]$  and CHI at pH 5.6 resulted in the formation of hydrogel in about 4 min (Figure 3A). Whereas 0.6 mM  $\text{Na}_2[\text{PdCl}_4]$  and CHI at pH 5.6 resulted in instantaneous hydrogel formation within about 30–40 s and no sol/gel conversion could be detected (Figure 3A). The metal coordinated complex formation reaction reaches equilibrium within 10 min for 0.4 and 0.6 mM  $\text{Na}_2[\text{PdCl}_4]$ , respectively. At concentrations of 0.05, 0.1 and 0.2 mM hydrogel formation at standard temperature and 5 °C did not occur (Figure 3B), but there was significant increase in viscosity and elasticity modulus within 10 min. Freezing 0.05 mM palladium complex, with 1.5% CHI that reached the equilibrium within 1 h at  $-12$  °C, did not result in sol gel transformation at these conditions (Figure 3). This correlates well with experimental data, when at least 24 h are required to prepare for CHI- $\text{Na}_2[\text{PdCl}_4]$  0.05 mM cryogel. Moreover, it is possible that the kinetics of the formation of this complex is slower, and therefore a long time is needed. Obtained hydrogels and cryogels are pH responsive and can easily dissolve under mild acidic conditions below pH 5.

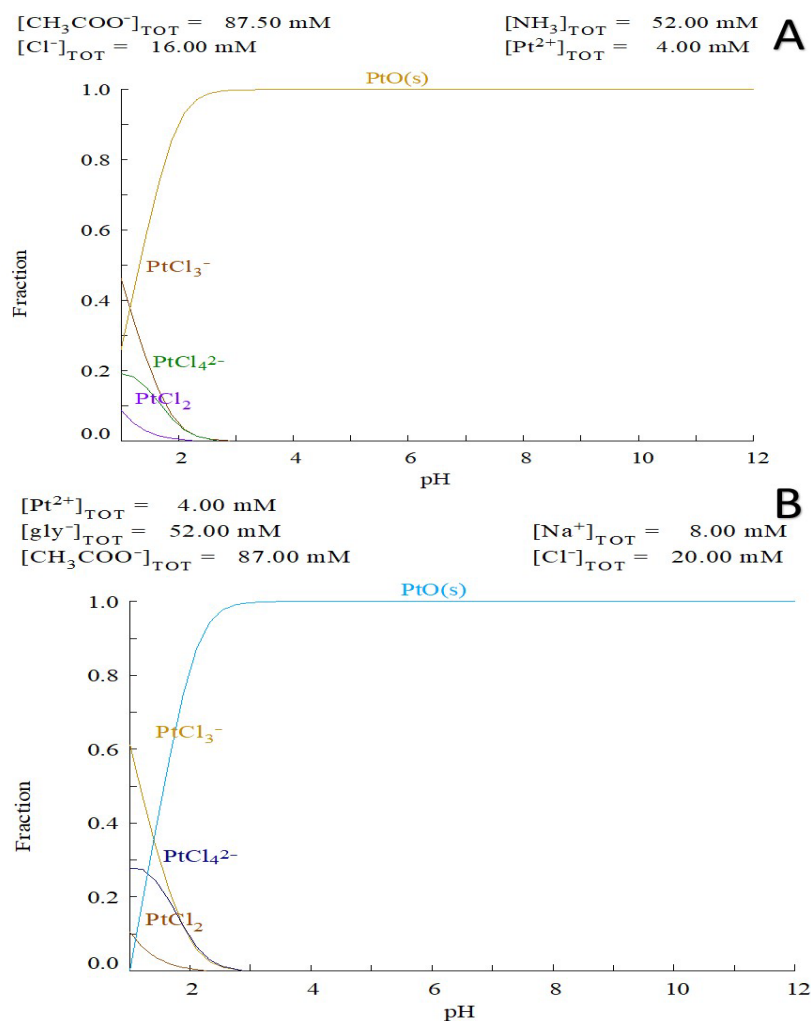


**Figure 2.** Speciation of Pt ions in reaction mixture: (A) 4 mM Pt(II) ions 52 mM ammonia, 87.5 mM of acetic acid and 16mM chloride anion vs. pH; (B) 4 mM Pt(II) ions 52 mM glycine, 87 mM of acetic acid and 20 mM chloride anion modeling vs pH(Diagram created by Medusa software).

Cryogels obtained with and without GA crosslinking were analyzed. The structural integrity of non-crosslinked GA cryogels was maintained by the formation of chelates between chitosan and  $[\text{PdCl}_4]^{2-}$  ions. Cryogels cross-linked by chelation (CHI- $[\text{PdCl}_4]^{2-}$ , containing 0.4 mM of the palladium complex) have elastic modulus of  $5.04 \pm 1.2 \text{ kPa}$  and  $5.8 \pm 1.5 \text{ kPa}$ , before and after swelling, respectively. After swelling, in water, ionic cryogels become more fragile and break easily compared to freshly prepared ones: therefore, the properties of the swollen CHI- $[\text{PdCl}_4]^{2-}$  sample were characterized as a cryogel with small pores and wide pore walls (Figure S5). Increasing the cross-linker concentration to 0.8 mM resulted in an efficient cross-linking of the gel, which had good viscoelastic properties and the sample did not break under compression up to at least 30% compression (Figure S5). The elasticity modulus of swollen in water CHI- $[\text{PdCl}_4]^{2-}$  cryogels with 0.2 mM and 0.6 mM of palladium was  $1.2 \pm 1.3 \text{ kPa}$  and  $4.7 \pm 2 \text{ kPa}$ , respectively. CHI- $[\text{PdCl}_4]^{2-}$  ionic cryogels with 0.4 mM palladium swollen in water break down at a compression stress of 3 kPa (Figure S5B). A freshly synthesized CHI- $[\text{PdCl}_4]^{2-}$  0.2 mM pH 4.7 can withstand compression stress up to 3–3.5 kPa (Figure S6C). Whereas freshly synthesized CHI- $[\text{PdCl}_4]^{2-}$  0.4 mM and 0.6 mM were elastic and showed no sign of breaking down up to 5.5 and 7 kPa, respectively (Figure S5A,C). The change in the mechanical properties after the swelling of the ionic cryogel in water or acidic buffered solution was observed, it becomes more fragile due to significant swelling of cryogel walls associated with a slow ligand

exchange in the non-covalent chelate, which ultimately resulted in a weaker gel. Moreover, after using  $[\text{PdCl}_4]^{2-}$  ions to form PdNP, the cryogel cross-linking will weaken, as well as gel strength. It can be concluded that the subsequent cross-linking with GA and the simultaneous reduction of Pd complexes to zero valent state should be carried out straight after the synthesis of the  $\text{CHI}-[\text{PdCl}_4]^{2-}$  cryogel in order to obtain a macroporous structure.

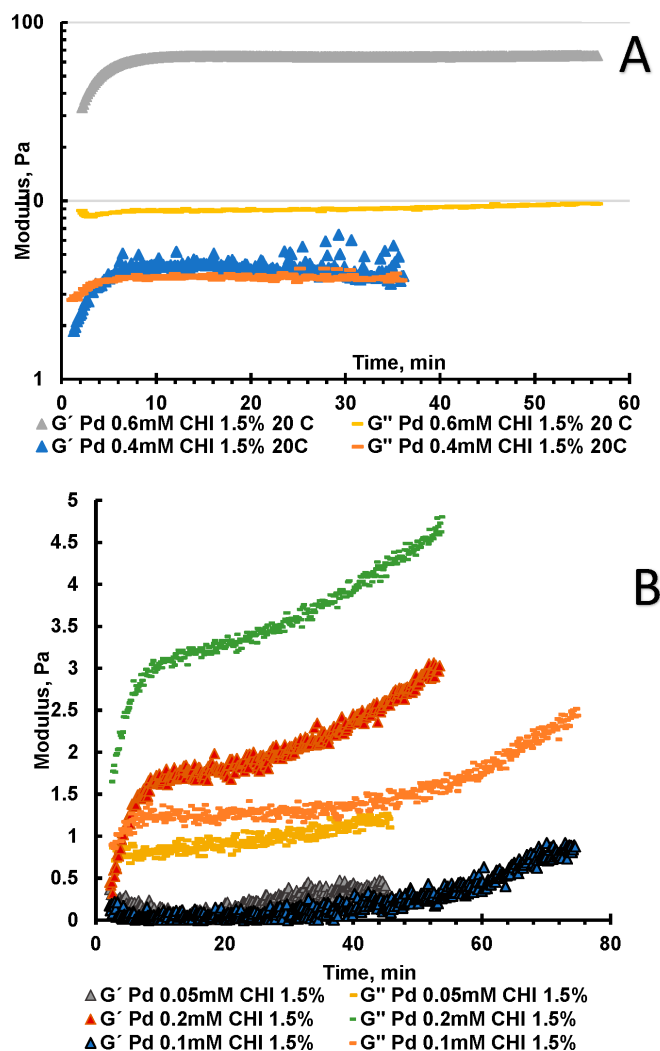


**Figure 3.** Monitoring the kinetic of formation and stability of gels using oscillatory shear rheology. Storage modulus,  $G'$ , and loss modulus,  $G''$ .  $G'$  and  $G''$  as a function of the shear stress amplitude  $\sigma$  for  $f = 1$  Hz: (A) Kinetics of  $\text{CHI}-[\text{PdCl}_4]$  0.4 mM and 0.6 mM hydrogel formation at pH 5.6 and 20 °C; (B) Kinetics of  $\text{CHI}-[\text{PdCl}_4]$  0.05 mM, 0.1 mM and 0.2 mM hydrogel formation at pH 5.6 and 20 °C.

A recent study illustrates that Pd and Pt complexes of organic amine and phosphine ligands resulted in systematically lower the reduction potential of the complex [34]. Thus, the redox potential  $E$  for  $[\text{PtBr}_4]^{2-}/\text{Pt}^0$  is +0.7 V, while the redox potential for  $[\text{Pt}(\text{NH}_3)_4]^{2-}/\text{Pt}$  is −0.14 V. It is known that  $E^0 \text{Pd}^{2+}/\text{Pd}^0$  is +0.951 V [35]. It was assumed that the obtained  $[\text{Pd}(\text{NH}_2\text{-CHI})_x\text{Cl}_y]^{2-}$  complexes have significantly smaller values, otherwise gel formation would not occur. The formation of gels in this case was confirmed by the rheology study (Figure 3). The kinetic of elastic modulus explains the stability of the  $\text{CHI}-[\text{Pt}(\text{NH}_3)_4]^{2-}$  complex under standard conditions, which did not get reduced easily, as it was observed in the case of CHI with gold complex. The gold complex was converted to AuNPs suspension under visible light exposure and mild heating [27]. The redox potential of the oxidation of an aldehyde to a carboxyl group is −0.58 V [36]. Thus, the covalent cross-linking of an ionic gel with GA can lead to a parallel reduction reaction resulting in

the formation of zerovalent metal and nanoparticles. Catalysis uses formic acid, which has a redox potential  $E^0 \text{CO}_2/\text{HCOOH} -0.61 \text{ V}$ , which ensures complete conversion of ionic noble metals into nanoparticles [37]. A similar, in situ approach of reduction Pd ions to carboxymethylcellulose stabilized PdNPs has previously been carried out using ascorbic acid and heating to  $95 \text{ }^\circ\text{C}$  [35].

In this work, a cryogel based on a biopolymer was used as a carrier for Pd and Pt catalysts. The CHI-GA-PdNPs cryogel has a macroporous structure of interconnected pores, which made it possible to pass a solution through it (Figure 4), thus the catalytic purification of water could be down in flow mode by passing solution through the cryogel made column. According to the analysis of TEM images using Image J software, the average size of PdNPs in the cryogel was 2.4 nm (Figure 4).

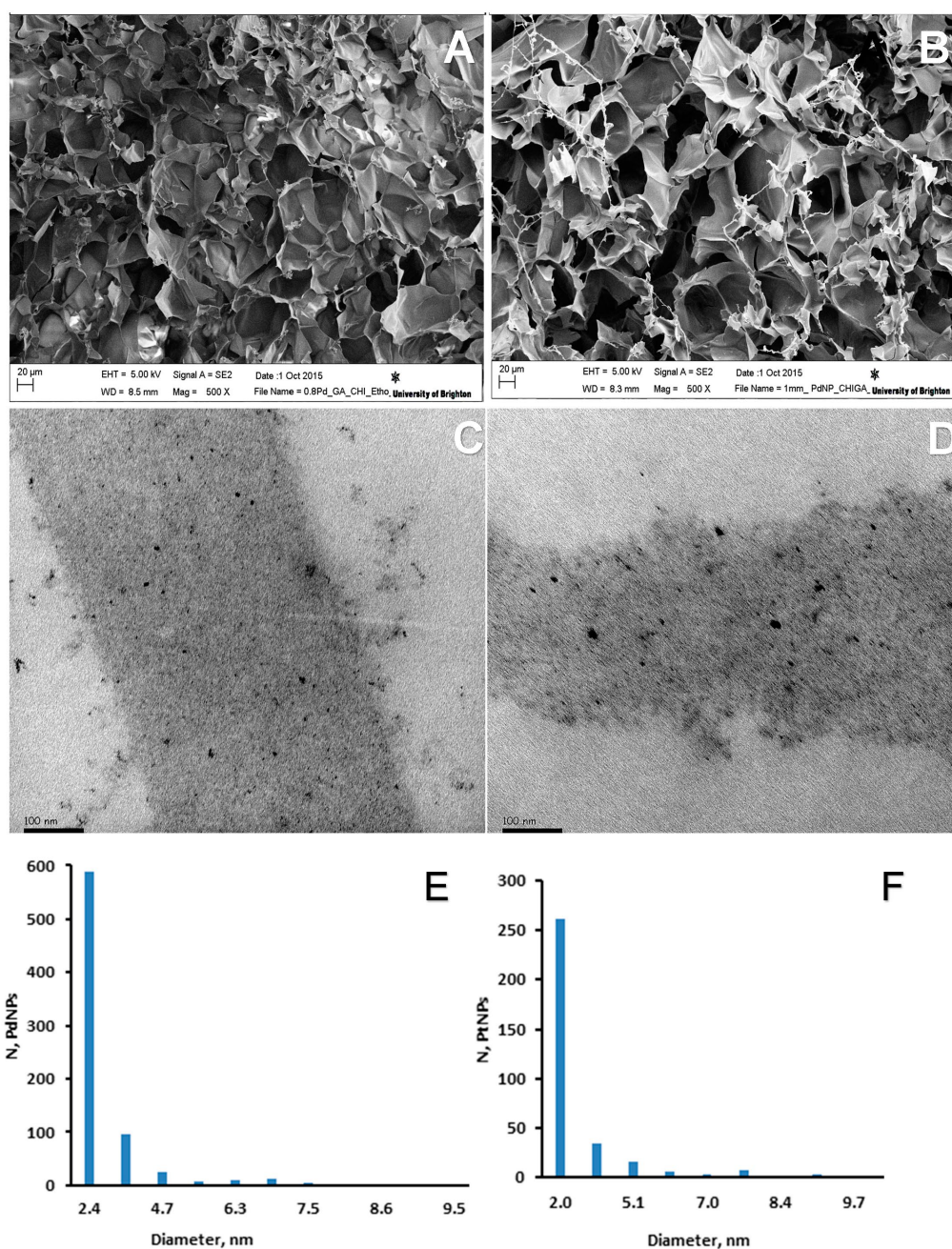


**Figure 4.** SEM images of CHI-GA-PdNPs cryogels: (A) 0.8 mM and (B) 1.0 mM; TEM images of cryogel walls: (C) CHI-GA-PdNPs 0.8 mM, (D) CHI-GA-PtNPs 4 mM; (E) PdNPs size distribution in CHI-GA-PdNPs 0.8 mM cryogel; (F) PtNPs size distribution in CHI-GA-PtNPs 4 mM cryogel.

Energy-dispersive X-ray spectroscopy analysis of CHI-GA-PdNPs confirmed the absence of PdNPs aggregates and good distribution of nanoparticles in the bulk of the cryogels walls, which is in good agreement with SEM images at high magnification (Figures 5 and S1). As expected, the chloride ions released during the formation of PdNPs act as counter ions to the protonated amino groups of chitosan. The higher PdNPs content, the higher the concentration of chloride ions was found, due to decomposition of  $[\text{PdCl}_4]^{2-}$  (Figure 5E,F).

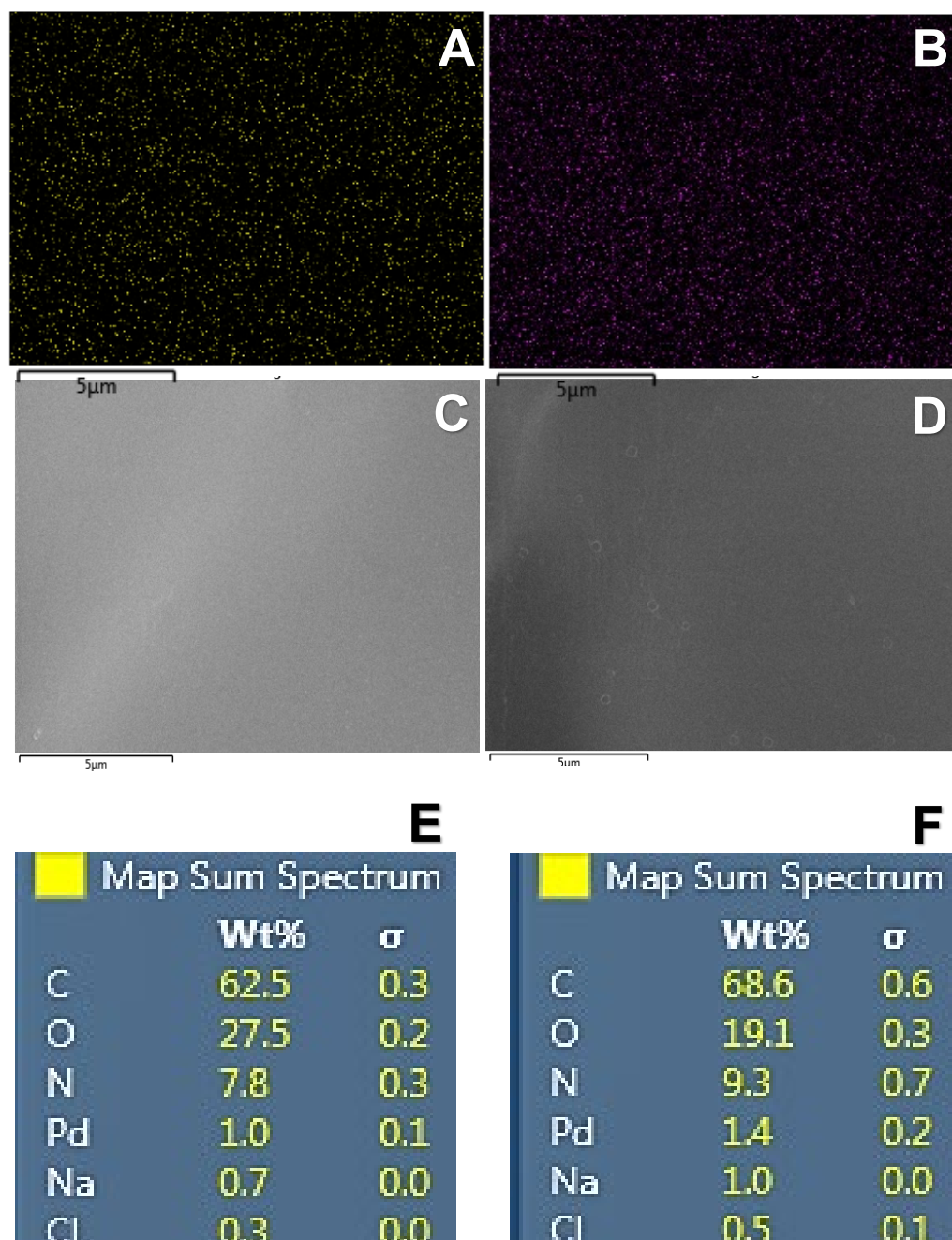


**Figure 5.** Energy-dispersive X-ray spectroscopy analysis of CHI-GA-PdNPs cryogel containing 0.8 mM PdNPs (A,C,E) and 1 mM PdNPs (B,D,F). Dots represent PdNPs (A,B).

The thermal stability of the catalyst is one of the important parameters. Decomposition of pure CHI occurred at 234 °C, and pure CHI completely decomposed at 450 °C with a weight loss of about 78%, which correlates with previous report [38]. The thermal stability of a dry hydrogel composed of CHI-GA and PdNPs correlates with the degradation

profile of pure CHI-GA cryogel in a nitrogen atmosphere. More detailed information regarding the GA cross-linked CHI was discussed previously [39]. The difference in the amount of solid residue after CHI-GA-PdNPs cryogel decomposition in air was 38% and 1.33%, for gels, containing 0.05 and 0.2 mM of Pd, respectively (Figures S2 and S3). PdNPs in the presence of air catalyze the oxidation of the polymer to CO<sub>2</sub>, whereas the cryogel with a low content of PdNPs seems to be more prone to carbonization. The 0.05 mM CHI-GA-PdNPs cryogel showed relative stability up to 235 °C compared to that containing 0.2 mM of Pd (Figures S2 and S3). Such a high temperature stability is explained by the significant crosslinking of chitosan with GA. The mass loss of CHI-GA-PdNPs cryogels in the temperature range from 100 °C to 235 °C in a nitrogen atmosphere can be associated with condensation and decarboxylation reactions (Figure S4). The weight loss of about 6–7% up to 100 °C was due to evaporation of chemically bonded water solvated by the polar groups of chitosan. Decomposition of 0.2 mM CHI-GA-PdNPs cryogel in air occurred at about 234 °C (Figure S3), and the sample degradation was completed at 325 °C with a weight loss of 96%. TGA thermograms of CHI-GA-PdNPs cryogels in air (Figure S5) showed that the degradation of CHI-GA-PdNPs 4 mM cryogels in air occurred at significantly lower temperatures, 212 °C, compared to the test carried out in an inert atmosphere (Figure S4). The cryogel completely decomposed at 290–300 °C with a weight loss of 98%. It appears that carbonization of CHI-GA-PdNPs 4 mM cryogels took place under heat treatment in nitrogen.

FTIR spectra of CHI-GA-PdNPs 0.2 mM and CHI-GA cryogels did not differ significantly, that may be attributed to the relatively low concentration of the noble metal. The only difference was the shift of the Schiff's base bond frequency, that overlapped with Amide II bond frequency at 1592 cm<sup>-1</sup> to 1589 cm<sup>-1</sup>, which can be related to coordination of these groups with Pd (Figure 6). As expected, the amino group bond at 1633 cm<sup>-1</sup> disappeared in CHI, when an excess of GA was used and full conversion to Schiff's base occurred (Figure 6). A frequency appeared at 1456 cm<sup>-1</sup> in CHI-GA-PdNPs and CHI-GA cryogel FTIR spectra related to –CH<sub>2</sub>– back bone of cross-linking agent [29,39].

### 3.2. Catalytic Activity of PdNPs Incorporated into Cryogels

The catalytic activity of CHI-GA-PdNPs cryogels was studied depending on the NP content, temperature, pH, and formic acid concentration in order to determine the most optimal conditions. Previously, it was shown, that a higher content of PdNPs led to a higher rate of contaminant degradation. It is known that for efficient degradation of chlorinated aromatic compounds catalyzed by PdNPs, it is necessary to use a 50-fold excess of formic acid [2]. The mechanism of degradation of chlorocompounds, when using formic acid involves first the decomposition of formic acid, which was discussed in detail earlier [15]. The literature data suggests pH-controlled reaction mechanisms (possibly H-atom and hydride transfer). Thus, formic acid acts as an H-donor for the de-chlorination reaction in aqueous solutions. H-consumers, such as chlorinated compounds, strongly stimulate the decomposition of formic acid. The half-life of 5 mg L<sup>-1</sup> chlorobenzene in the presence of 1 mg L<sup>-1</sup> PdNPs is about 120 s under optimal reaction conditions [15]. For PdNPs supported on Ni the optimal pH values for degradation of chlorinated aromatic compounds was about 3 and 4 [2]. In this work, similar conditions were used, such as concentration of formic acid and the ratio of formic acid to substrate. UV-visible spectroscopy was used to measure concentration of 2CP. Samples of the reaction mixture were taken after incubation of cryogels in a 2CP solution for a certain time and the absorbance was monitored at 280 nm. The control experiment of the de-chlorination process was carried out similarly to the experiment described above without PdNPs in the cryogel. As expected, there was no adsorption of chlorophenol on the cryogel matrix due to the hydrophilic nature of the cryogel. The degradation of chlorophenol reached 50% within one hour, after which a slight decrease in catalyst activity was observed, regardless of the catalyst content (Figure 7).

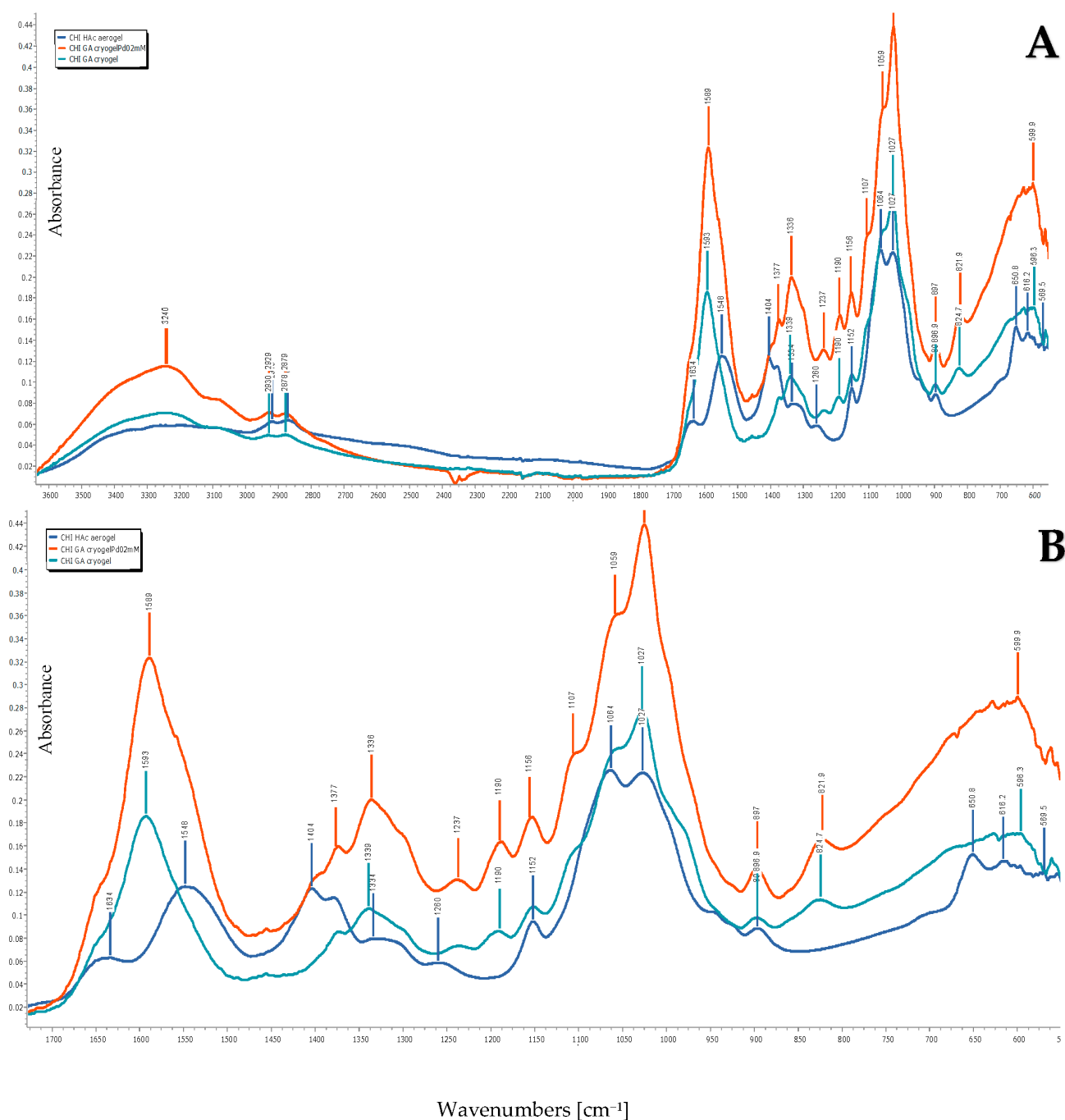


**Figure 6.** FTIR spectra of freeze dried cryogels CHI-GA-PdNPs 0.2 mM; cryogels CHI-GA and CHI dissolved in acetic acid in the wavenumber range of: (A) 3700–600 cm<sup>-1</sup>; (B) 1800–600 cm<sup>-1</sup>.

A recent report found a significant correlation between the PdNPs size (2.1–4.5 nm) on activated carbon (Pd/AC) and the kinetic rate of formic acid decomposition [40]. The formic acid is disproportionate in a catalytic dehydrogenation reaction to form hydrogen and carbon dioxide, however, this reaction can proceed according to a different mechanism with the formation of carbon monoxide and water. It is well known that CO deactivates the catalysts [41,42], this could be a reason of the slowing degradation in this case as well. The use of low reaction temperatures in the range of 25 to 60 °C improves the stability of the Pd/AC catalyst and therefore the reaction temperature of the formic acid decomposition should be  $T < 60$  °C [41,42]. It also was found that deactivated Pd/AC can be regenerated to its original activity by drying overnight at 60 °C [42].

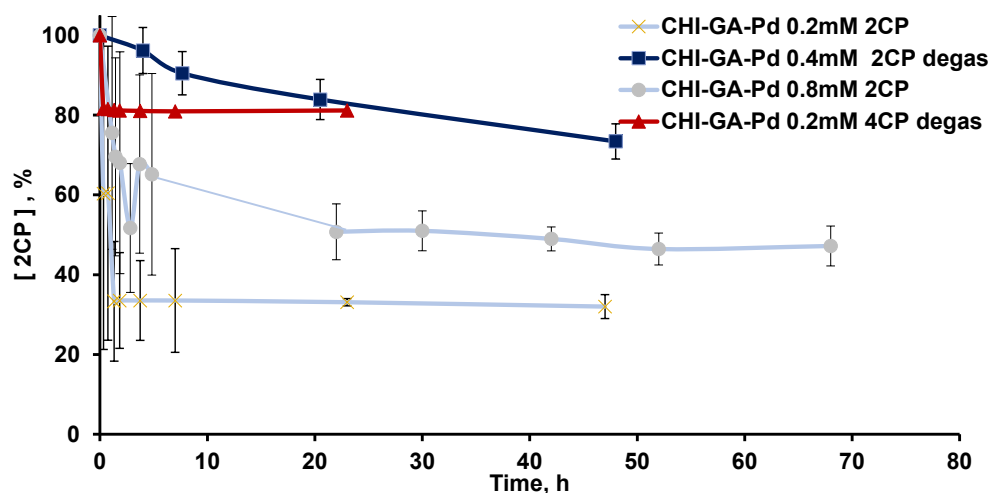


**Figure 7.** Kinetic curves of chlorophenols (50 ppm) decomposition catalyzed by CHI-GA-PdNPs without degassing of the reaction mixture, UV-vis monitoring PdNPs-CHI-GA 0.2 mM (4.9  $\mu\text{g}$  PdNPs) and 0.8 mM (45  $\mu\text{g}$  PdNPs) and PdNPs-CHI-GA 0.2 mM after additional degassing applying vacuum of reaction mixture at time point 16 h.

GC-MS and HPLC analysis was used to monitor the kinetics of the catalytic decomposition process. According to the literature data, chlorophenols are reduced to benzene, phenol, and cyclohexanone [31]. The reference solution acquired in Single Ion Monitoring and the 2 most abundant ions of 2CP were monitored ( $m/z$  128 and 130) (Figures S7 and S8). 2CP degradation catalyzed by CHI-GA-PdNPs 0.8 mM showed only 50% conversion within two hours (Figure 8A). In another experiment with CHI-GA-PdNPs 0.4 mM (21  $\mu\text{g}$  PdNPs) the UV reading indicated the presence of the substrate, while the GC-MS data confirmed the formation of phenol, and therefore the UV absorbance did not change significantly due to overlap of substrate and product absorption (Figure S9). Most likely, other products with adsorption at 280 nm could be formed during de-chlorination process, but due to limited access to standards only concentration of chlorophenols, benzene and phenol was monitored. Incomplete CP conversion and reduced phenol formation were noted, which may be related to subsequent reduction in compounds, but no products were identified (Figure S9).

4CP degradation was tested using CHI-GA-PdNPs 0.2 mM cryogels (4  $\mu\text{g}$  PdNPs), showing a similar trend towards incomplete conversion, and only 40% contaminants were removed within 100 min (Figure S11). It was assumed that this observation may be due to chloride ions accumulation, which could poison catalysts, but this has not been previously reported. The possibility to recycle the catalyst was also checked, but the reaction of hydrodehalogenation was not sufficient and comparable to 1st cycle (Figure S11A). Further optimization of the catalyst regeneration conditions (shock heat treatment, chemical treatment, etc.) is necessary after evaluation of the mechanism of poisoning.

To test the hypothesis of poisoning by released chloride ions, the reaction was carried out in the presence of silver ions, which should lead to the precipitation of silver chloride and eliminating chloride ions from the system. The kinetic rate of the reaction in presence of silver was similar to that of reduction with sodium borohydride (Figure 9). The control experiment of mixing 2CP with silver nitrate did not result in a shift or absorbance intensity of 2CP over a few hours. Thus, this reaction setup did not lead to a significant improvement in the conversion rate and may be costly for real life application (Figures 9 and S12). This may be due to the fact that AgCl crystals were precipitated on PdNPs blocking the active catalytic site. Increasing the reaction temperature to 80  $^{\circ}\text{C}$  led to a significant acceleration, showing that the conversion efficiency of 2,4-dichlorophenol reached 85% and 73% within 42.5 h, respectively (Figures 9 and S13). Nevertheless, after several hours of reaction, the hydrodechlorination reaction self-terminated, resulting in a 40% decrease in

the concentration of 2,4-dichlorophenol at pH 3 at ambient temperature. Most likely, this is due to the accumulation of carbon monoxide, which blocks active sites of the catalyst. As recently reported, at 85 °C, a side reaction of the decomposition of formic acid proceeds in the form of the formation of carbon monoxide, which poisons the catalyst [42]. Increasing the pH of reaction mixture to 6.2 did not improve the conversion degree. Increasing the temperature to 80 °C accelerated the 2CP decomposition reaction with an efficiency of 67% in 24 h and 85% for 42.5 h compared to 25% conversion at room temperature (Figure 9). The control experiment for the hydrogenation of 2CP using borohydride confirms that the catalyst is active at standard conditions of the hydrogenation process without significant catalyst poisoning. However, the use of borohydride had some drawbacks, such as the formation of gas bubbles in the cryogel structure, which can change the diffusion of the substrate and affect the kinetics during long-term use. Increasing the formic acid concentration to a ratio of 1:100 to the substrate (40 mM) accelerated the reaction at 80 °C (Figure 9).

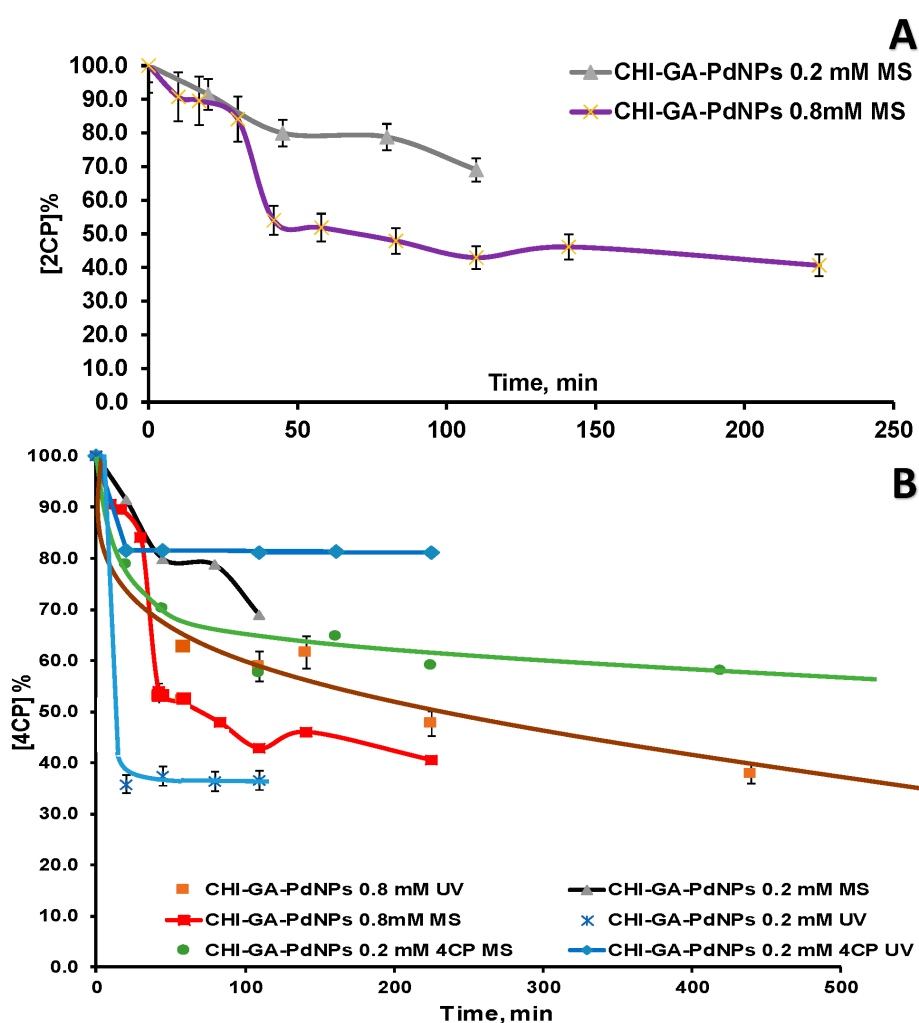


**Figure 8.** Kinetic curves of chlorophenols (50 ppm) decomposition in a batch mode in presence of CHI-GA-PdNPs 0.2 mM (4.9  $\mu$ g PdNPs) and 0.8 mM (44.8  $\mu$ g PdNPs) cryogels and formic acid (20 mM): (A) 2CP was monitored by GC-MS; (B) 4CP was monitored by GC-MS and UV spectroscopy.

It can be assumed that self-termination after several hours occurred due to the accumulation of carbon monoxide onto PdNPs, or due to the formation of cyclohexanone, which immediately interacts with primary amino groups of CHI and therefore change the microenvironment, blocking the subsequent diffusion of the contaminant to the PdNPs surface. The complete catalytic conversion of the selected chlorophenols was not achieved, which

can be due to poisoning on the mechanism similar to previously reported, but the study of the mechanism was beyond the scope of this work and was not further investigated.

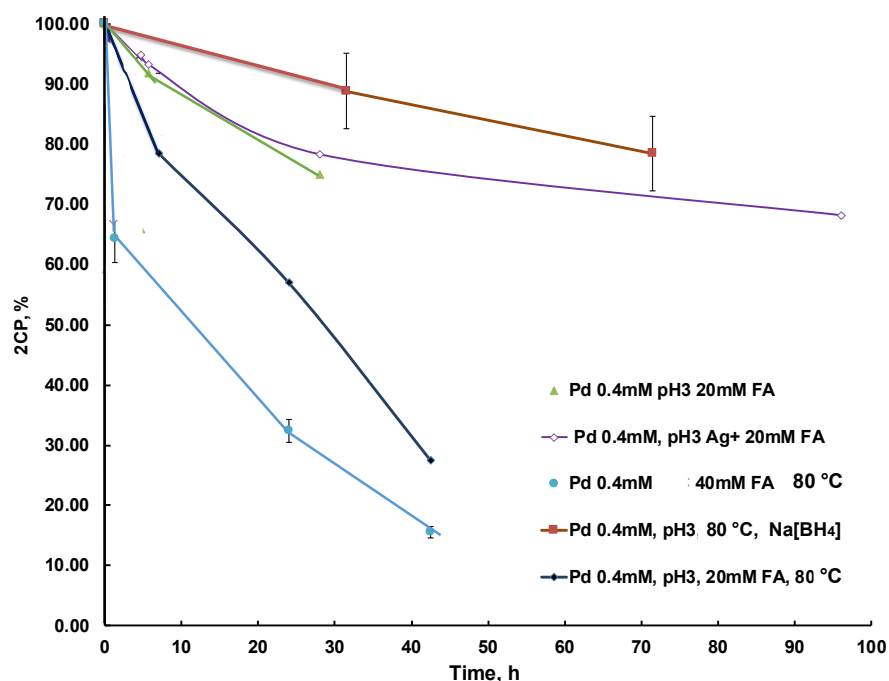


**Figure 9.** Kinetic curves of catalytic 2CP decomposition in the presence of CHI-GA-PdNPs 0.4 mM (21  $\mu\text{g}$  PdNPs) cryogels in a batch mode at various parameters: added Ag, formic acid concentration, temperature and pH. The reaction mixture: 2CP (51.2 ppm), formic acid (20 mM), and pH 3. The concentration of contaminant was measured using HPLC.

It was observed that at pH 3 the chlorophenol conversion was comparable between catalysts CHI-GA-PdNPs 0.4 mM (21  $\mu\text{g}$ ) and CHI-GA-PtNPs 1 mM (97.5  $\mu\text{g}$  PtNPs) reaching 80 and 90%, respectively (Figure 10A), assuming that the average particles distribution was comparable. pH is an important factor that can affect the efficiency of substrate diffusion to the nanoparticle and adsorption/desorption from the catalyst surface. Cryogel based on CHI-GA at pH 3 is positively charged, which is associated with the protonation of primary amino groups [43]. While chlorophenols have a pKa value of about 9.5–10 and therefore are not charged at pH 3 and 6 [44]. The CHI-GA cryogel at pH 6.2 has an almost neutral charge due to existence of most amino groups in unprotonated state, therefore, the probability of stronger adsorption of chlorophenols on the CHI-GA scaffold due to hydrogen bonds is high.

The lower the metal concentration was used, the smaller average particle size was and the higher efficiency of the catalyst. A similar trend was illustrated for 0.5 mM AuNPs catalyst during the nitrophenol reduction [29]. PdNPs (31.9  $\mu\text{g}$ ) within CHI-GA-PdNPs 0.4 mM cryogel showed an approximately 100-fold higher rate of catalytic hydrogenation process at pH 6 compared to 390  $\mu\text{g}$  of PtNPs in the CHI-GA-PtNPs 4 mM cryogel (Figure 10B), which is consistent with other studies. Thus, the hydrodechlorination of 4CP in stirred tank reactor using Pd, Pt, and Rh immobilized on  $\gamma$ -alumina (0.5% *w/w*) under mild reaction conditions (20–40  $^{\circ}\text{C}$ ) showed that Pd and Rh were more catalytically active than Pt [45]. Recently, a Pd/carbon nanotube (CNT)-Ni foam microreactor system was successfully tested for the rapid and efficient (99%) hydrogenation process using formic acid [46]. Another study states that catalytic hydrodechlorination of 4CP occurs in an aqueous solution of formic acid with an efficiency of 92% within 2 h using 3 g/L of Pd/Ni catalyst [2]. Most probably the support plays a significant role in the activity of PdNPs, moreover, the shape of the particles can affect the activity. In case of 2,4DiClPh, the termination of the reaction was faster compared to monochlorophenols (Figures 7 and S15).

HPLC chromatograms confirmed numerous products of 2,4DiClPh hydrogenation with retention time in the range of 2.5–12 min (Figures 10B, S12–S14). The mechanism of this reaction has been described previously. Adsorption of 2,4DiClPh or phenol equilibrium was reached within 5 min for 2,4DiClPh. Phenol has a low adsorption capacity on PdNPs deposited on hollow fiber membranes and a high transfer rate. The order of rates was  $k_3 \gg k_1 \gg k_2$ , indicating that the predominant route was sequential de-chlorination without desorption of monochlorophenols. Approximately 70% of 2,4DiClPh was dechlorinated to phenol followed by stepwise de-chlorination with 2-CP at 26% and 4-CP at 4%. Due to the dominant reaction, there is no desorption of 2-CP or 4-CP, their accumulation of monochlorophenols in the reaction mixture was small after 5 min [47]. The de-chlorination of 2,4DiClPh occurred in two steps: (a) 2,4DiClPh adsorption to PdNP, with activation of the C-Cl bond; and (b) C-Cl bond breaking coupled electron-transfer from activated H that also was adsorbed to the PdNPs. They found that adsorption configuration with two Cl atoms bonded to Pd(0) is favorable based on its largest  $\Delta E_{\text{ads}}$ , compared with single *para* or *ortho* Cl bonds with Pd atoms [47].

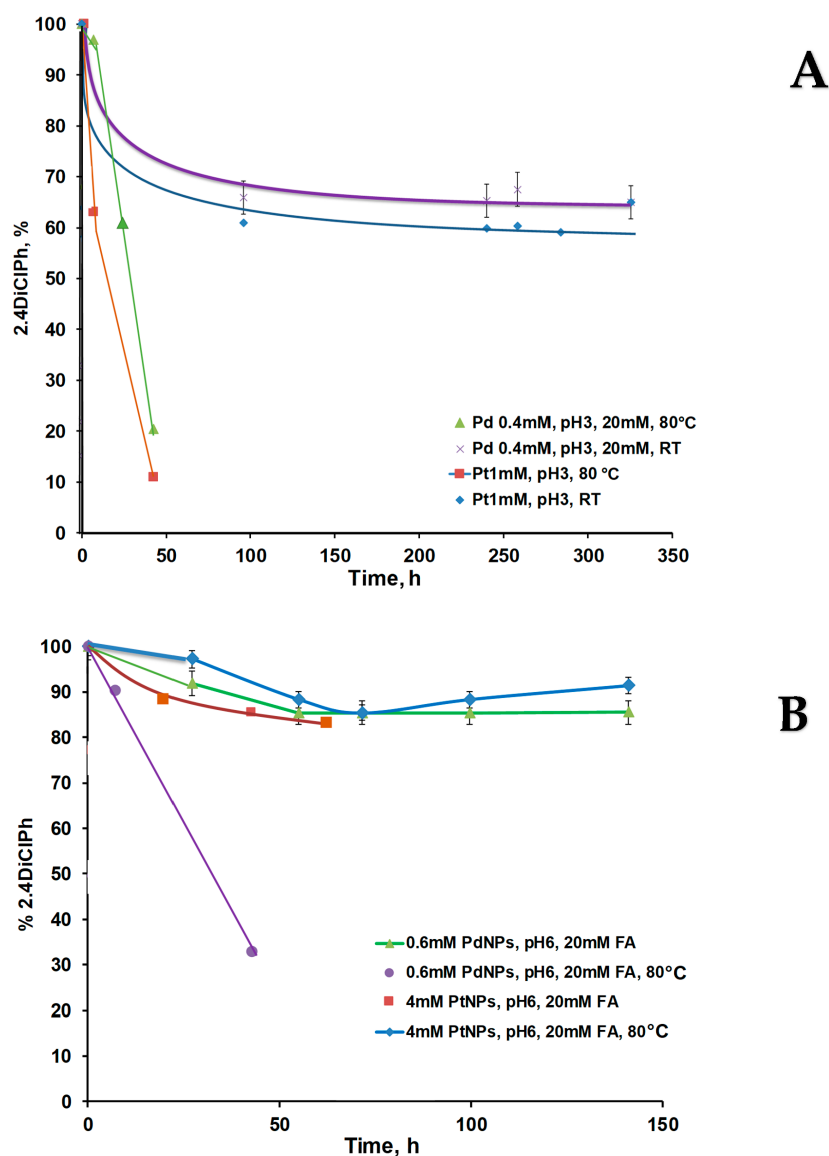


**Figure 10.** Kinetic curves of 2,4DiClPh de-chlorination process in batch mode in the presence of CHI-GA-PdNPs and CHI-GA-PtNPs cryogels at room temperature or at 80 °C The mixture of 2,4DiClPh (65.2 ppm) and formic acid (20 mM) at: (A) pH 3 and; (B) pH 6.2.

The combination of factors to proceed the reaction with silver nitrate at 80 °C in formic acid was not tested because it can form AgNPs which can influence the reaction and also use chlorophenols as a reducing agent. The complex formation between 2,4-Di-CIPh and silver ions or unexpected new products were not observed (Figure S15C). The HPLC chromatogram of the reaction mixture with silver nitrate contained significantly less side products detectable at 280 nm compared to the reaction mixture without silver ions (Figures S15 and S12). This may indicate the participation of silver redox reactions with these compounds. The control experiment demonstrated no leakage of other compounds from the CHI-GA-PdNP scaffold (Figure S13). Chlorophenols adsorption were not observed for CHI-GA and CHI-GA-PdNPs cryogel. A recent report shows that the rate of Pd-catalyzed electrochemical hydrodechlorination of chlorinated compounds is significantly lower (25 times) than the rate of hydrodechlorination carried out using hydrogen gas. In aqueous solution of pH 7, a substantial part of 4-CP ( $pK_a = 8.6$ ) exists in its anionic form on the surface of cathode. Therefore, the negative surface potential of the Pd/Ni foam will decrease the concentration of adsorbed 4-CP, which can significantly reduce the rate of the hydrodechlorination reaction [48]. Specific catalyst activities for Pd/ $Al_2O_3$  was up to  $A_{Pd} = 200 \text{ L g}^{-1} \text{ min}^{-1}$  in clean water. Hydrodechlorination kinetics of 3-chlorobiphenyl (3-CBP) by Pd/ $Al_2O_3$  in water (pH = 8.3,  $c_{0,3\text{-CBP}} = 2.5 \text{ mg L}^{-1}$ ,  $c_{\text{catalyst}} = 125 \text{ mg L}^{-1}$ ) a specific catalyst activity was determined of about  $190 \text{ L g}^{-1} \text{ min}^{-1}$  [49]. Hydrophobic coating of PdNPs by silicone polymers was successful in protecting the Pd sites against ionic catalyst poisons. Thus, catalyst activities measured with hydrophobically modified catalysts was equaled to  $A_{Pd} \approx 80$  to  $2.3 \text{ L g}^{-1} \text{ min}^{-1}$  in comparison to unprotected Pd/ $Al_2O_3$  catalysts in long-term usage under field conditions results in  $A_{Pd} \approx 0.05 \text{ L g}^{-1} \text{ min}^{-1}$  [49]. All this could be further considered for the improvement catalyst performance.

#### 4. Conclusions

A macroporous catalyst based on chitosan with entrapped PdNPs and PtNPs was prepared by primary crosslinking via formation of metal chelates, followed by simultaneous covalent crosslinking and metal reduction with glutaraldehyde. This makes it possible to form a stabile macroporous polymer matrix with in situ-formed PdNPs with a size 2–3 nm, which are preferable for catalytic reaction. The catalytic activity of noble metal nanoparticles remains after inclusion into the polymer structure. The catalyst proved to be effective for the hydrodehalogenation of 4-chlorophenol, 2-chlorophenol and 2,4-dichlorophenol using environmentally friendly and safe reducing agents, formic acid. Formic acid has advantages over sodium borohydride because no gas is generated during the reaction, which can inhibit the reaction in the porous material in long-term use. The study of various conditions showed that the reaction was more efficient at 40 mM formic acid, pH 3 and a temperature of 80 °C. CHI-GA-PtNP cryogels showed lower catalytic activity compared to CHI-GA-PdNP cryogels under comparable conditions at pH 6. The observed termination of the hydrodechlorination of chlorophenols by in situ synthesized supported PdNPs associated with poisoning of the catalyst with CO and chlorine ions is discussed. Overall, the study opened several fundamental questions in understanding the mechanism of the catalytic reaction and the stability of the catalysts.

**Supplementary Materials:** The following supporting information can be downloaded at: <https://www.mdpi.com/article/10.3390/inorganics11010023/s1>, Figure S1: Energy-dispersive X-ray spectra; Figures S2–S4: TGA of cryogels; Figures S5–S6: compression test of ionic cryogels; Figure S7: chlorophenols calibration curves; Figures S8–S10: kinetics of hydrochlorination process monitoring using GC-MS; Figure S11: kinetics of hydrochlorination process monitoring using UV-vis; Figures S12–S15: HPLC chromatograms of the reaction mixture at different experimental settings.

**Author Contributions:** Conceptualization, D.A.B.; Methodology, D.A.B.; Formal Analysis, I.N.S.; Investigation, D.A.B.; Resources, I.N.S.; Data Curation, D.A.B.; Writing—Original Draft Preparation, D.A.B.; Writing—Review and Editing, D.A.B. and I.N.S.; Visualization, D.A.B.; Project Administration, I.N.S. and D.A.B. All authors have read and agreed to the published version of the manuscript.

**Funding:** This research was funded by Marie Skłodowska-Curie Actions Individual Fellowship grant 2016–2018 “Cryobacteria-reactor” N701289 and British Council and Newton—Al-Farabi Partnership Programme: Researcher Links Travel Grant N172701258, 2015.

**Data Availability Statement:** Not applicable.

**Acknowledgments:** The Marie Skłodowska-Curie Actions Individual Fellowship grant “Cryobacteria-reactor” N 701289 and British Council and Newton—Al-Farabi Partnership Programme: Researcher Links Travel Grant N172701258 for the support of the research. Royal Society International Exchanges 2019 Cost Share scheme grant for the support of time while manuscript writing.

**Conflicts of Interest:** Authors declare no conflict of interest.

## References

1. Syafrudin, M.; Kristanti, R.A.; Yuniarto, A.; Hadibarata, T.; Rhee, J.; Al-Onazi, W.A.; Algarni, T.S.; Almarri, A.H.; Al-Mohaimed, A.M. Pesticides in drinking water—A review. *Int. J. Environ. Res. Public Health* **2021**, *18*, 468. [[CrossRef](#)] [[PubMed](#)]
2. Wang, S.; Yang, B.; Zhang, T.; Yu, G.; Deng, S.; Huang, J. Catalytic hydrodechlorination of 4-chlorophenol in an aqueous solution with Pd/Ni catalyst and formic acid. *Ind. Eng. Chem. Res.* **2010**, *49*, 4561–4565. [[CrossRef](#)]
3. Igbinosa, E.O.; Odjajare, E.E.; Chigor, V.N.; Igbinosa, I.H.; Emoghene, A.O.; Ekhaie, F.O.; Igiehon, N.O.; Idemudia, O.G. Toxicological profile of chlorophenols and their derivatives in the environment: The public health perspective. *Sci. World J.* **2013**, *2013*, 460215. [[CrossRef](#)]
4. World Health Organization. *A Global Overview of National Regulations and Standards for Drinking-Water Quality*; WHO: Geneva, Switzerland, 2021.
5. Khan, M.; Khan, M.A.; Khan, Q.; Habibi-Yangjeh, A.; Dang, A.; Maqbool, M. Review on the hazardous applications and photodegradation mechanisms of chlorophenols over different photocatalysts. *Environ. Res.* **2021**, *195*, 110742.
6. Garba, Z.N.; Zhou, W.; Lawan, I.; Xiao, W.; Zhang, M.; Wang, L.; Chen, L.; Yuan, Z. An overview of chlorophenols as contaminants and their removal from wastewater by adsorption: A review. *J. Environ. Manag.* **2019**, *241*, 59–75. [[CrossRef](#)] [[PubMed](#)]
7. Chi, N.; Xu, W. Synthesis of TiO<sub>2</sub>/gC 3N<sub>4</sub> Hybrid Photocatalyst and its Application for Degradation of Chlorophenol as Organic Water Pollutant. *Int. J. Electrochem. Sci* **2022**, *17*, 2.
8. Chen, X.; Ning, X.-a.; Lai, X.; Wang, Y.; Zhang, Y.; He, Y. Chlorophenols in textile dyeing sludge: Pollution characteristics and environmental risk control. *J. Hazard. Mater.* **2021**, *416*, 125721. [[CrossRef](#)]
9. Kumar, D.; Sharma, C. Reduction of chlorophenols and sludge management from paper industry wastewater using electrocoagulation process. *Sep. Sci. Technol.* **2020**, *55*, 2844–2854. [[CrossRef](#)]
10. Pozan, G.S.; Boz, I. Hydrodechlorination of 2, 3, 5-trichlorophenol in methanol/water on carbon supported Pd-Rh catalysts. *Environ. Eng. Sci.* **2008**, *25*, 1197–1202. [[CrossRef](#)]
11. World Health Organization. *Guidelines for Drinking-Water Quality: First Addendum to the Fourth Edition*; WHO: Geneva, Switzerland, 2017.
12. Chang, W.; Kim, H.; Lee, G.Y.; Ahn, B.J. Catalytic hydrodechlorination reaction of chlorophenols by Pd nanoparticles supported on graphene. *Res. Chem. Intermed.* **2016**, *42*, 71–82. [[CrossRef](#)]
13. Le, X.; Dong, Z.; Li, X.; Zhang, W.; Le, M.; Ma, J. Fibrous nano-silica supported palladium nanoparticles: An efficient catalyst for the reduction of 4-nitrophenol and hydrodechlorination of 4-chlorophenol under mild conditions. *Catal. Commun.* **2015**, *59*, 21–25. [[CrossRef](#)]
14. Ruiz-García, C.; Heras, F.; Calvo, L.; Alonso-Morales, N.; Rodríguez, J.; Gilarranz, M. N-doped CMK-3 carbons supporting palladium nanoparticles as catalysts for hydrodechlorination. *Ind. Eng. Chem. Res.* **2019**, *58*, 4355–4363. [[CrossRef](#)]
15. Kopinke, F.-D.; Mackenzie, K.; Koehler, R.; Georgi, A. Alternative sources of hydrogen for hydrodechlorination of chlorinated organic compounds in water on Pd catalysts. *Appl. Catal. A: Gen.* **2004**, *271*, 119–128. [[CrossRef](#)]
16. Shu, X.; Yang, Q.; Yao, F.; Zhong, Y.; Ren, W.; Chen, F.; Sun, J.; Ma, Y.; Fu, Z.; Wang, D. Electrocatalytic hydrodechlorination of 4-chlorophenol on Pd supported multi-walled carbon nanotubes particle electrodes. *Chem. Eng. J.* **2019**, *358*, 903–911. [[CrossRef](#)]
17. Hu, R.; Li, C.; Wang, X.; Sun, Y.; Jia, H.; Su, H.; Zhang, Y. Photocatalytic activities of LaFeO<sub>3</sub> and La<sub>2</sub>FeTiO<sub>6</sub> in p-chlorophenol degradation under visible light. *Catal. Commun.* **2012**, *29*, 35–39. [[CrossRef](#)]
18. Xia, S.; Zhang, X.; Zhou, X.; Meng, Y.; Xue, J.; Ni, Z. The influence of different Cu species onto multi-copper-contained hybrid materials’ photocatalytic property and mechanism of chlorophenol degradation. *Appl. Catal. B: Environ.* **2017**, *214*, 78–88. [[CrossRef](#)]
19. Sekula jr, P.; Bačik, M.; Mosej, J.; Sekula sr, P.; Berillo, D.; Zeng, Y.; Kupka, D.; Václavíková, M.; Ivaničová, L. Elimination of 2-chlorophenol by two types of iron particles. *Mater. Today: Proc.* **2018**, *5*, 22889–22893. [[CrossRef](#)]
20. Molina, C.; Calvo, L.; Gilarranz, M.; Casas, J.; Rodríguez, J. Hydrodechlorination of 4-chlorophenol in aqueous phase with Pt–Al pillared clays using formic acid as hydrogen source. *Appl. Clay Sci.* **2009**, *45*, 206–212. [[CrossRef](#)]

21. Berillo, D.A.; Caplin, J.L.; Cundy, A.B.; Savina, I.N. A cryogel-based bioreactor for water treatment applications. *Water Res.* **2019**, *153*, 324–334. [[CrossRef](#)]
22. Al-Jwaid, A.K.; Berillo, D.; Savina, I.N.; Cundy, A.B.; Caplin, J.L. One-step formation of three-dimensional macroporous bacterial sponges as a novel approach for the preparation of bioreactors for bioremediation and green treatment of water. *RSC Adv.* **2018**, *8*, 30813–30824. [[CrossRef](#)]
23. Wang, Z.; Liao, Y.; Liu, J.; Huang, X. On-site separation and enrichment of heavy metal ions in environmental waters with multichannel in-tip microextraction device based on chitosan cryogel. *Microchem. J.* **2022**, *175*, 107107. [[CrossRef](#)]
24. Purohit, S.; Chini, M.K.; Chakraborty, T.; Yadav, K.L.; Satapathi, S. Rapid removal of arsenic from water using metal oxide doped recyclable cross-linked chitosan cryogel. *SN Appl. Sci.* **2020**, *2*, 768. [[CrossRef](#)]
25. Yin, M.; Li, X.; Liu, Y.; Ren, X. Functional chitosan/glycidyl methacrylate-based cryogels for efficient removal of cationic and anionic dyes and antibacterial applications. *Carbohydr. Polym.* **2021**, *266*, 118129. [[CrossRef](#)]
26. Fan, M.; Gong, L.; Huang, Y.; Wang, D.; Gong, Z. Facile preparation of silver nanoparticle decorated chitosan cryogels for point-of-use water disinfection. *Sci. Total Environ.* **2018**, *613*, 1317–1323. [[CrossRef](#)]
27. Berillo, D.; Mattiasson, B.; Kirsebom, H. Cryogelation of chitosan using noble-metal ions: In situ formation of nanoparticles. *Biomacromolecules* **2014**, *15*, 2246–2255. [[CrossRef](#)]
28. Berillo, D.; Cundy, A. 3D-macroporous chitosan-based scaffolds with in situ formed Pd and Pt nanoparticles for nitrophenol reduction. *Carbohydr. Polym.* **2018**, *192*, 166–175. [[CrossRef](#)]
29. Berillo, D. Gold nanoparticles incorporated into cryogel walls for efficient nitrophenol conversion. *J. Clean. Prod.* **2020**, *247*, 119089. [[CrossRef](#)]
30. Akpınar, F.; Evli, S.; Güven, G.; Bayraktaroğlu, M.; Kilimci, U.; Uygün, M.; Aktaş Uygün, D. Peroxidase immobilized cryogels for phenolic compounds removal. *Appl. Biochem. Biotechnol.* **2020**, *190*, 138–147. [[CrossRef](#)]
31. Calvo, L.; Gilarranz, M.; Casas, J.; Mohedano, A.; Rodríguez, J. Hydrodechlorination of 4-chlorophenol in water with formic acid using a Pd/activated carbon catalyst. *J. Hazard. Mater.* **2009**, *161*, 842–847. [[CrossRef](#)]
32. Berillo, D.A.; Dyusebaeva, M.A. Synthesis of hydrazides of heterocyclic amines and their antimicrobial and spasmolytic activity. *Saudi Pharm. J.* **2022**, *30*, 1036–1043. [[CrossRef](#)]
33. Vasily, D.S.; Alexei, A.T.; Nina, P.K. Platinum Complexes with Bioactive Nitroxyl Radicals: Synthesis and Antitumor Properties. In *Nitroxides*; Alexander, I.K., Ed.; IntechOpen: Rijeka, Croatia, 2012; Chapter 14; pp. 385–406.
34. Yadav, V.; Jeong, S.; Ye, X.; Li, C.W. Surface-Limited Galvanic Replacement Reactions of Pd, Pt, and Au onto Ag Core Nanoparticles through Redox Potential Tuning. *Chem. Mater.* **2022**, *34*, 1897–1904. [[CrossRef](#)]
35. He, F.; Liu, J.; Roberts, C.B.; Zhao, D. One-step “green” synthesis of Pd nanoparticles of controlled size and their catalytic activity for trichloroethene hydrodechlorination. *Ind. Eng. Chem. Res.* **2009**, *48*, 6550–6557. [[CrossRef](#)]
36. Loach, P.A. Oxidation-reduction potentials, absorbance bands and molar absorbance of compounds used in biochemical studies. In *Handbook of Biochemistry and Molecular Biology*; CRC Press: Boca Raton, FL, USA, 2010; pp. 557–563.
37. Wu, J.; Huang, Y.; Ye, W.; Li, Y. CO<sub>2</sub> reduction: From the electrochemical to photochemical approach. *Adv. Sci.* **2017**, *4*, 1700194. [[CrossRef](#)]
38. Kumar, D.; Kumar, P.; Pandey, J. Binary grafted chitosan film: Synthesis, characterization, antibacterial activity and prospects for food packaging. *Int. J. Biol. Macromol.* **2018**, *115*, 341–348. [[CrossRef](#)]
39. Pieróg, M.; Ostrowska-Czubenko, J.; Gierszewska-Drużyńska, M. Thermal degradation of double crosslinked hydrogel chitosan membranes. *Prog. Chem. Appl. Chitin Its Deriv.* **2012**, *17*, 71–78.
40. Li, J.; Chen, W.; Zhao, H.; Zheng, X.; Wu, L.; Pan, H.; Zhu, J.; Chen, Y.; Lu, J. Size-dependent catalytic activity over carbon-supported palladium nanoparticles in dehydrogenation of formic acid. *J. Catal.* **2017**, *352*, 371–381. [[CrossRef](#)]
41. Hu, C.; Pulleri, J.K.; Ting, S.-W.; Chan, K.-Y. Activity of Pd/C for hydrogen generation in aqueous formic acid solution. *Int. J. Hydrog. Energy* **2014**, *39*, 381–390. [[CrossRef](#)]
42. Martin, C.; Quintanilla, A.; Vega, G.; Casas, J.A. Formic acid-to-hydrogen on Pd/AC catalysts: Kinetic study with catalytic deactivation. *Appl. Catal. B: Environ.* **2022**, *317*, 121802. [[CrossRef](#)]
43. Chen, T.; Kumar, G.; Harris, M.T.; Smith, P.J.; Payne, G.F. Enzymatic grafting of hexyloxyphenol onto chitosan to alter surface and rheological properties. *Biotechnol. Bioeng.* **2000**, *70*, 564–573. [[CrossRef](#)]
44. Liptak, M.D.; Gross, K.C.; Seybold, P.G.; Feldgus, S.; Shields, G.C. Absolute p K<sub>a</sub> determinations for substituted phenols. *J. Am. Chem. Soc.* **2002**, *124*, 6421–6427. [[CrossRef](#)]
45. Diaz, E.; Casas, J.A.; Mohedano, A.F.; Calvo, L.; Gilarranz, M.A.; Rodríguez, J.J. Kinetics of the hydrodechlorination of 4-chlorophenol in water using Pd, Pt, and Rh/Al<sub>2</sub>O<sub>3</sub> catalysts. *Ind. Eng. Chem. Res.* **2008**, *47*, 3840–3846. [[CrossRef](#)]
46. Xiong, J.; Ma, Y. Catalytic hydrodechlorination of chlorophenols in a continuous flow Pd/CNT-Ni foam micro reactor using formic acid as a hydrogen source. *Catalysts* **2019**, *9*, 77. [[CrossRef](#)]
47. Wu, C.; Zhou, L.; Zhou, Y.; Zhou, C.; Xia, S.; Rittmann, B.E. Dechlorination of 2, 4-dichlorophenol in a hydrogen-based membrane palladium-film reactor: Performance, mechanisms, and model development. *Water Res.* **2021**, *188*, 116465. [[CrossRef](#)]

48. Zhang, Y.; Yu, C.; Hu, X.; Yu, J.; Mao, Z.; Wu, H.; Shi, M.; Liu, Q.; Xu, Y. Why does Pd-catalyzed electrochemical hydrodechlorination proceed much slower than hydrodechlorination using hydrogen gas? *Electrochim. Acta* **2021**, *390*, 138770. [[CrossRef](#)]
49. Kopinke, F.-D.; Angeles-Wedler, D.; Fritsch, D.; Mackenzie, K. Pd-catalyzed hydrodechlorination of chlorinated aromatics in contaminated waters—Effects of surfactants, organic matter and catalyst protection by silicone coating. *Appl. Catal. B: Environ.* **2010**, *96*, 323–328. [[CrossRef](#)]

**Disclaimer/Publisher’s Note:** The statements, opinions and data contained in all publications are solely those of the individual author(s) and contributor(s) and not of MDPI and/or the editor(s). MDPI and/or the editor(s) disclaim responsibility for any injury to people or property resulting from any ideas, methods, instructions or products referred to in the content.